Surface Science 421 (1999) 320–336

Atomistics of the epitaxial growth of Cu on W(110)

K. Reshöft [a], C. Jensen [b], U. Köhler [b,*]

[a] *Institut für Experimentelle und Angewandte Physik, Christian-Albrechts-Universität Kiel, Olshausenstraße 40, D-24098 Kiel, Germany*
[b] *Institut für Experimentalphysik, Oberflächenphysik, Ruhr-Universität Bochum, D-44780 Bochum, Germany*

Received 9 April 1998; accepted for publication 3 November 1998

Abstract

Time-resolved in situ STM has been used to study the epitaxial growth of Cu on W(110) at temperatures ranging from room temperature up to 300°C. Sequences of STM images directly show the atomistics of the growth process on the surface. Additionally, SPA-LEED has been used to obtain precise information about the lateral geometrical dimensions of the different developing Cu structures. A sequence of three different structures is needed to transfer the Cu film to its intrinsic fcc-like behavior. The first layer of Cu on W(110) grows pseudomorphically in a fractal geometry. According to this growth behavior strain effects are considered to play a predominant role. With the second Cu layer a strained structure originates which is divided into small domains by a periodic trench network. A structure model for this double layer is suggested. Depending on the deposition conditions the trench network is decorated by a complex chain structure of third layer islands. Beginning with the completion of the third layer a periodic dislocation network appears. This structure can be attributed to an fcc Cu(111) layer with a slightly expanded surface unit mesh. Beyond the fourth layer a Cu on Cu(111) growth is established, which is only slightly affected by the underlying transition layer. Higher temperature deposits show an incomplete triple layer with a nearly perfect chain structure indicating that a relaxed third layer is metastable. Cu in excess grows in wedge-shaped 3D Stranski–Krastanov islands with atomically smooth (111) surfaces even on a misoriented substrate. © 1999 Elsevier Science B.V. All rights reserved.

Keywords: Copper; Epitaxy; Tungsten

1. Introduction

The misfit as well as the difference in the crystal structure between the substrate and an epitaxial layer often dominate the properties of thin heteroepitaxial layers. It may lead to a number of different structural defects depending on the coverage, temperature and growth rate. Quite often the adlayer initially adopts the lattice constant and the crystal structure of the substrate. At a certain coverage, the adlayer begins to compensate for the increasing mechanical strain energy by the creation of misfit dislocations [1]. While the geometrical arrangement of these dislocations can easily be determined for thick layers, the exact mechanism and the atomic scale details of their creation in the initial stages are quite often unknown. We were able to observe these processes in detail using time-resolved, in situ STM measurements, i.e. taking STM images directly during the course of MBE growth. In this publication we focus on the heterosymmetric system Cu on W(110) (W shows a bcc lattice with a lattice constant of $a_W = 3.165$ Å, bulk Cu a fcc lattice with $a_{Cu} = 3.615$ Å, see Fig. 1), which has a possible application as a spacer layer

* Corresponding author. Fax: +49-234-7094173;
e-mail: ulrich.k.koehler@rz.ruhr-uni-bochum.de.

PII: S0039-6028(98)00859-0

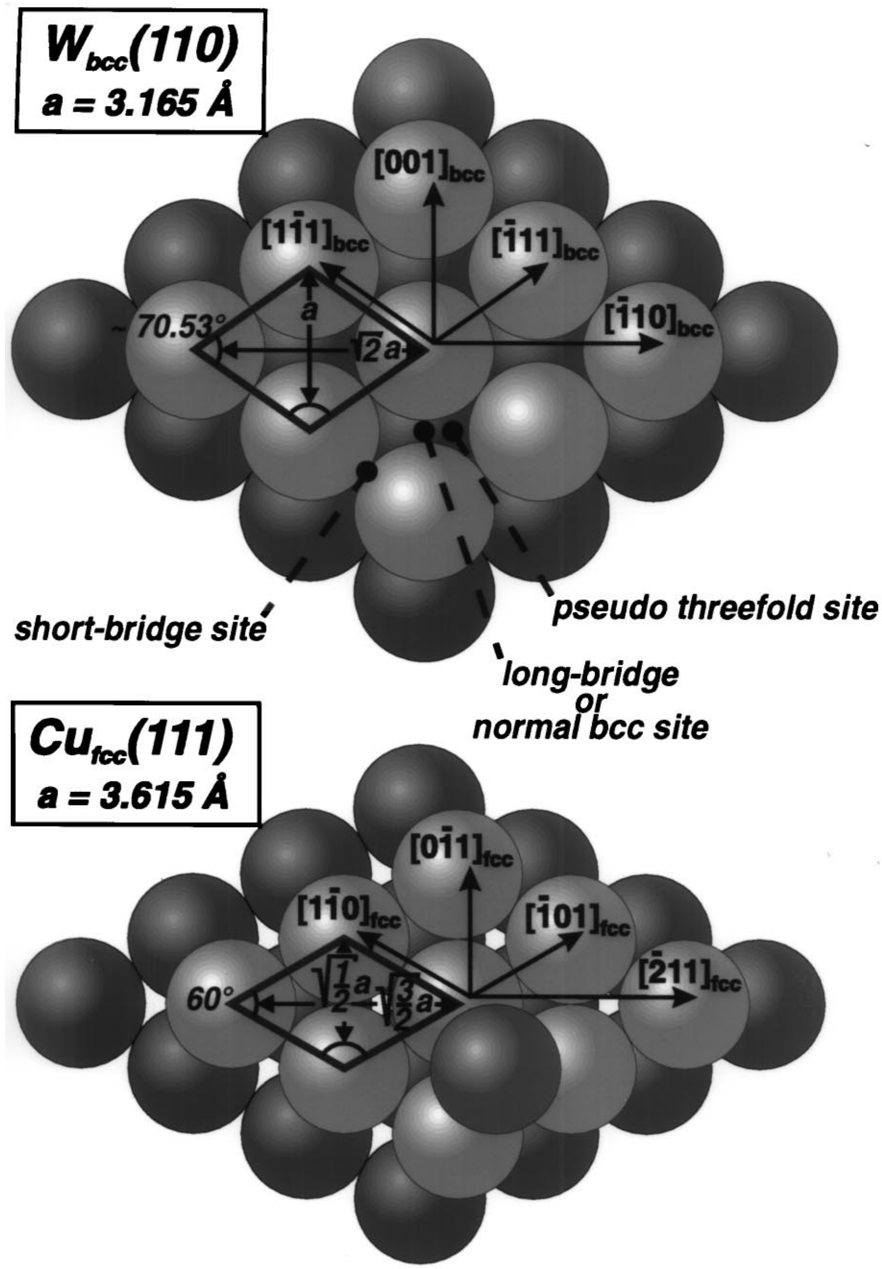

Fig. 1. Schematic representations of the bcc (110) surface of W and the fcc (111) surface of Cu, relatively oriented in Nishiyama–Wassermann-x configuration. Three highly symmetrical sites for adsorbate atoms on the W surface are marked.

in magnetic sandwich and multilayers [2] or as a bimetallic substrate for catalytic reactions [3]. The known characteristics of the geometrical structure of this system are based essentially on LEED, AES [4–7], RHEED [8], He diffraction [9], SPLEEM [10] and LEEM experiments [11] giving only surface averaging or wide range information about structural transitions with increasing coverage.

Therefore little is known about the exact atomic arrangement of the first few monolayers. The goal of the present publication is on the one hand to give an overview of the phenomena found by an in situ STM study and on the other hand to provide detailed information on the coverage dependence of the growth behavior on an atomic level, especially for the coverage between one and four monolayers, where the relaxation of the thin Cu film takes place.

2. Experimental

The experiments were performed in an ion-pumped UHV chamber equipped with a scanning tunneling microscope, SPA-LEED optics, a quadrupole mass spectrometer and an Auger spectrometer. The W(110) substrate was oriented with a deviation less than 0.2° from (110), mechanically polished and electropolished in 1% NaOH. After bakeout the crystal was cleaned by many (~ 50) heating–cooling cycles from 2000 K (8 s) down to 300 K in 5×10^{-7} mbar O_2 atmosphere to remove the residual carbon contamination. Subsequently, about five heating–cooling cycles from 2100 K (8 s) to 300 K were used to remove O_2 and other adsorbates. The last sequence was repeated before each Cu deposition. The sample was mounted on a transferable sample holder with integrated electron beam heater. Cu was evaporated from an Al_2O_3 crucible with a growth rate ranging from 0.006 to 3 monolayers per minute. With careful outgassing a working pressure below 1×10^{-10} mbar could be reached during the in situ time-resolved measurements, which were performed with an evaporator pointing at an angle of $\sim 15°$ with respect to the surface plane onto the sample located in the STM. For additional static measurements Cu was evaporated ex situ from an external evaporator at normal incidence. Elevated substrate temperatures in the STM experiments were accomplished by radiative heating with a tungsten filament immediately behind the sample.

The time-resolved STM measurements were performed in situ by taking snapshots of the same area of the sample every 1 or 2 min directly during evaporation. This procedure enables us to follow an initially chosen, specific location on the surface through the different stages of growth on an atomic level. Possible shadow effects caused by the scanning tip have been reduced by retracting the tip a few thousand Å every time between acquisition of successive frames. The sequences of STM micrographs shown in this paper are selected frames from sequences containing 28–215 single STM images. The coverage Θ as indicated in the figures was measured by determining the covered area directly in the images without consideration whether the layers are pseudomorphic or relaxed (apparent coverage). All STM images were obtained in the constant current mode at currents of 1–3 nA and sample bias voltages between -200 and 200 mV.

3. Results and discussion

3.1. Overview

Fig. 2 presents an outline of the epitaxial growth of Cu on W(110) up to a thickness of several monolayers (ML). The section of the sample is the same in all STM images. The images are selected from a sequence taken during the growth at an elevated temperature of 80°C with an average apparent coverage ranging from $\Theta=0$ up to $\Theta\approx6$ ML (beginning with nucleation of the eighth layer in the highest covered region). The growth process starts with the nucleation of Cu islands exhibiting a fractal geometry within the first ML (a). Subsequently the uncovered gaps in the layer are filled until a closed first ML of Cu is formed (d). The second ML starts to grow on top of the first one also in a fractal but more compact geometry (e). In contrast to the first layer there is now a strong preference of the growth towards the $[001]_{bcc}$ direction with respect to the substrate. It is remarkable that, once a second layer area has formed, immediately third layer patches sit on top. With the completion of the second layer (g) these patches join in long narrow chains which again are oriented in $[001]_{bcc}$ direction. The degree of ordering of this structure is not very perfect, i.e. the chains are winding and sometimes split. After the macroscopic completion of the second layer

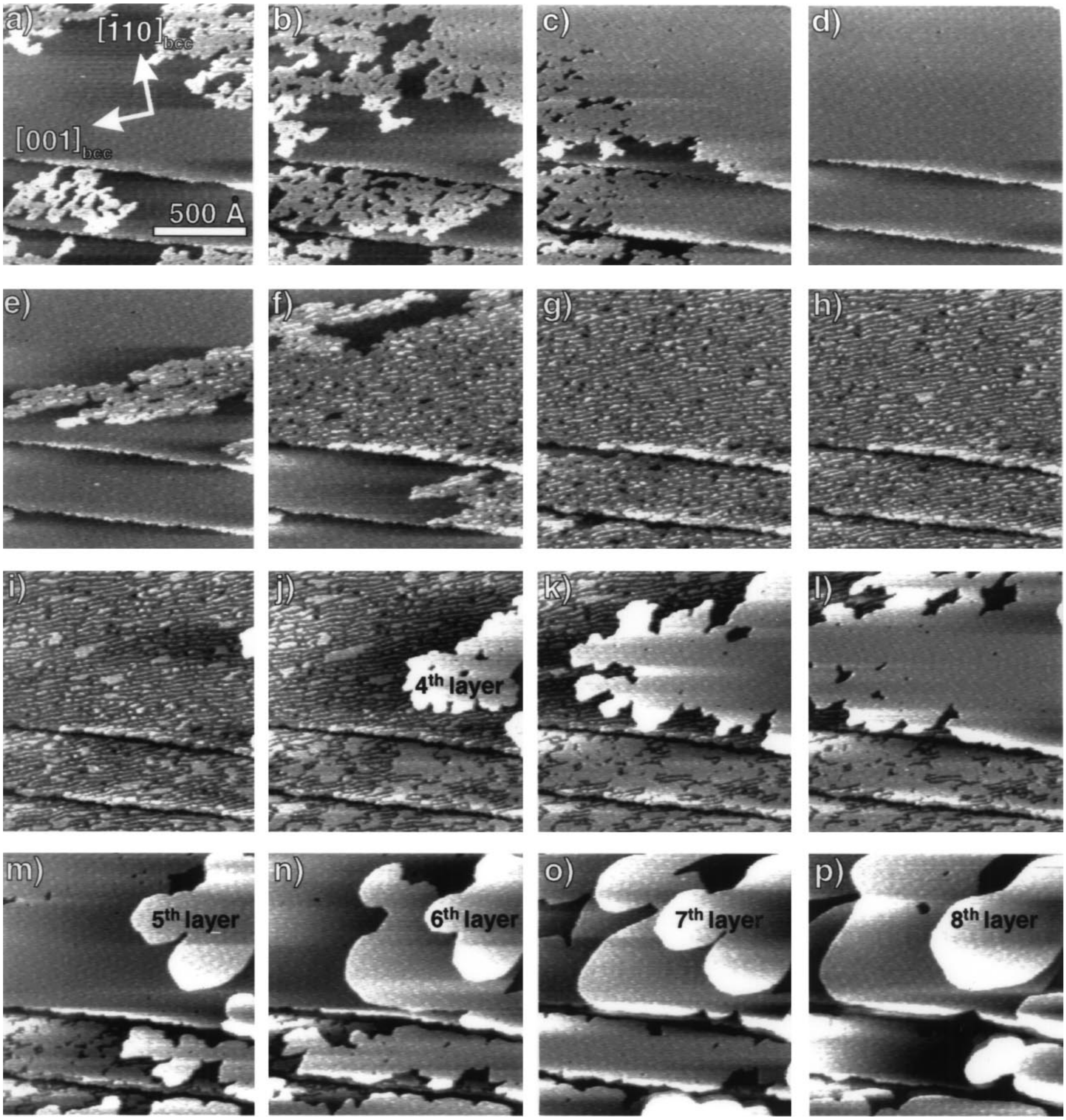

Fig. 2. Selected frames from a sequence of STM images of the epitaxial growth of Cu on W(110), prepared in situ at 80°C. The figure shows the same area of the sample as a function of time.

with a lot of small vacancies remaining, it comes to an increased filling of gaps between neighboring chains leading to a statistical distribution of third layer islands (i). Again exhibiting a fractal growth front, the fourth layer always starts to grow a long time before the third layer is completed (j). Therefore the formation of the coherent dense fourth layer includes a simultaneous filling of third layer gaps underneath. Seen as a movie picture sequence, the fourth layer growth process appears as a wetting-like spreading with a preferred covering of filled third layer areas. Beyond the fourth layer the growth mode changes to a typical Cu on Cu(111) like growth exhibiting compact island shapes with a closed growth front (m–p). The island edges exhibit a hexagonal outline corresponding to the hexagonal symmetry of the fcc (111) surface oriented in Nishiyama–Wassermann-x configuration [12] on top of the W(110) substrate.

It has to be remarked that the scanned section of Fig. 2 shows an inhomogeneous coverage throughout the whole movie. The reason for this is a relatively blunt tip, compared with the size of the section, which partly led to a screening of the atomic Cu beam during the scanning process. As a result, the average Cu flux was slightly reduced from the top of the right-hand side to the left bottom, and also in carrying out the tip retracting procedure described above this effect could not be completely compensated. The pattern which can be seen on closed layers is due to electronic noise caused by the heating of the sample and must not be interpreted as a physical feature.

After this overview we now turn to a full discussion dealing with finer details of the nucleation process, the occurrence of dislocation networks in the second, third and fourth layers and possible models of the atomic arrangement. We start with the first layer and subsequently focus on the next higher layers.

3.2. First layer

Fig. 3 presents STM images from a sequence showing the nucleation process and room temperature (RT) growth of Cu on W(110) in the submonolayer range in more detail. The coverage ranges up to $\Theta = 0.35$ ML.

In Fig. 3a five Cu islands have nucleated on a single terrace. The number of islands does not increase in the following, indicating that in this stage, at a coverage of 0.01 ML, the nucleation phase is already completed. The initial growth rate, leading to this island density of about 1/500 000 Å^{-2} was about 0.0004 ML s^{-1}. At 0.35 ML the island diameter is about 800 Å (Fig. 3l), in agreement with Ref. [9], in which a diameter of more than 100 Å at 0.5 ML is suggested. As already mentioned, the islands show an irregular two-dimensional fractal growth without a preferred orientation, which is accomplished by a chaining of small compact clusters with an diameter of 25–35 Å. This fractal growth of clusters is different from that described by the theory of diffusion limited aggregation of single atoms, presented by Witten and Sanders [13,14]. The formation of these clusters can be understood as a consequence of a high binding energy of Cu atoms attaching to an island edge only within an initially formed cluster below a certain limiting size. The existence of such a limit in cluster size, on the other hand, could be explained by a lowering of the stress energy to some extent due to an inward relaxation of the Cu atoms at the edges of the pseudomorphic clusters. Initially a cluster is formed around a nucleation center by incorporation of atoms. When approaching the limiting size the increasing inward relaxation of Cu atoms at the step edge leads to a weaker bonding to the cluster. Finally no additional Cu atoms can be incorporated any more. From this point on further growth proceeds by forming additional clusters connected by narrow bridges. These connected cluster arrays are formed by the attachment of single Cu atoms nucleating at existing clusters, the diffusion of existing clusters has never been observed. Diffusion along the step edges of the individual clusters making up the Cu islands is possible but the formation of a compact island shape is strongly suppressed.

With increasing deposition temperature the separation of the islands and therefore also the maximum island diameter increases from about 500 Å at RT to about 1300 Å at 150°C. This indicates that the mobility of the Cu atoms on the W substrate increases with temperature. The 'dendricity' of the island, on the other hand, does not change significantly up to 250°C, again pointing to a stress limitation effect as the driving force for the fractal island shape. Consistently, thermal annealing of the fractal islands up to 250°C results in only a small scale smoothing of the individual

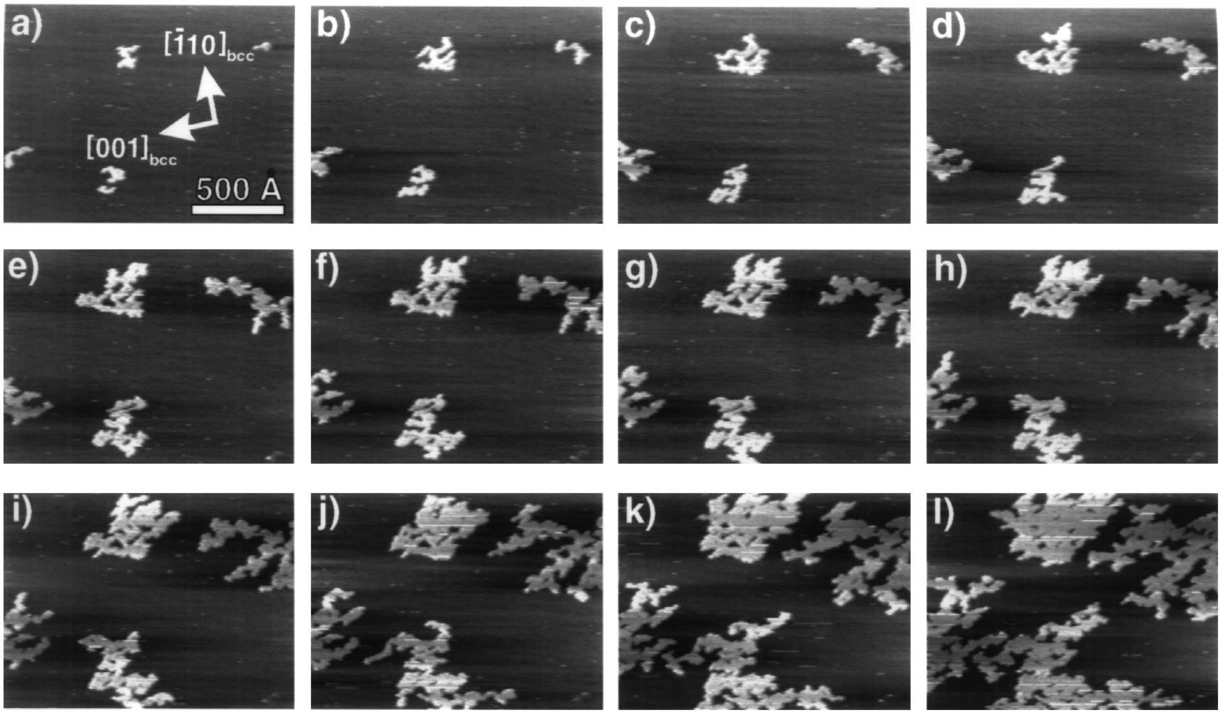

Fig. 3. Selected frames from a sequence of STM images showing the nucleation of first layer fractals of Cu on W(110) at RT up to a coverage of ($\Theta = 0.35$ ML).

clusters making up the islands. Even annealing for hours does not lead to a compact island shape.

Also at step edges growth proceeds in a fractal mode at RT. No compact stripe is formed as seen e.g. in Fig. 4b and c. As in the case of the islands on the terrace, no change in the fractal appearance at step edges is found up to 250°C. The secondary role of a kinetic limitation is proposed as well by Mo and Himpsel [15], who found no change in the roughness of the Cu stripe at step edges even after thermal annealing at temperatures as high as 400°C. On the other hand, on Mo(110) Cu forms smooth stripes at the step edge at elevated temperature enabling possible applications as one-dimensional nano-wires [17–19]. Cu atoms attaching to islands or to substrate steps experience competing driving forces. The minimization of the energy stored in Cu steps, on the one side, favors large islands or stripes with straight step edges. The minimization of the misfit strain, on the other side, favors the formation of small islands. Whereas on W(110) the first driving force dominates, on Mo(110) the latter wins. A possible explanation for this difference can be found in the stronger lateral bonding in the Cu adlayer on Mo(110) (compared with W(110)) [16] which increases the step energy for Cu on Mo(110) and therefore straightens the step edges. In the same way the fractal growth mode of Cu on W(110) at the step edges (as seen in Fig. 4) has been suggested as a two-dimensional analogy of the three-dimensional Stranski–Krastanov growth mode. The step edge is first covered by one closed row of Cu atoms, and further growth proceeds in separate islands only weakly attached to the step edge [19].

The growth of fractals, as can be seen from the sequence in Fig. 3 is very unequally distributed. For example, there is no formation of any arms at the bottom of the upper left island (d–k), while in the meantime the upper right island extends three large arms. This may be because for the formation of a cluster a definite number of impinging atoms (critical cluster) is necessary. This process would be a statistical event, which is preferred in regions,

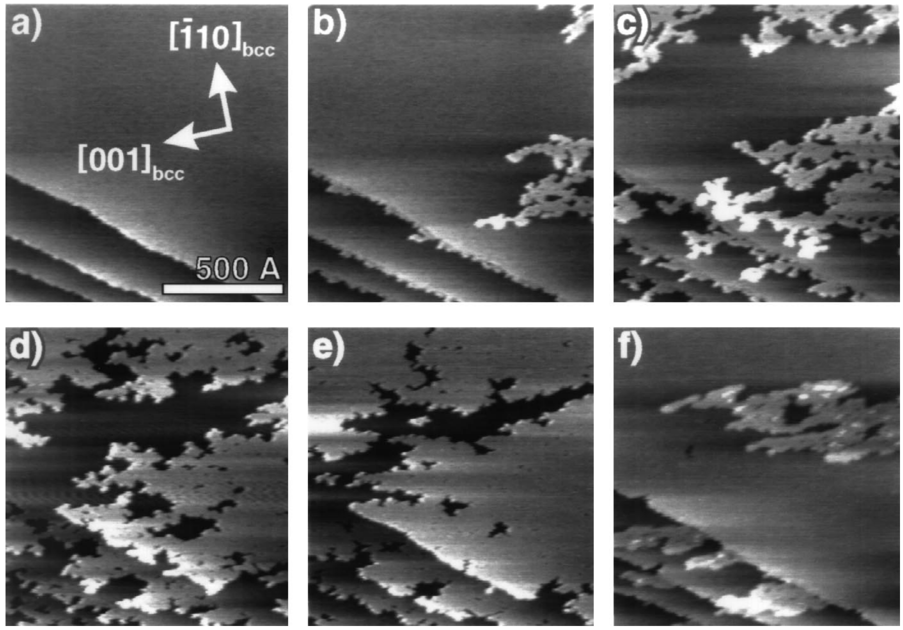

Fig. 4. Sequence of STM images showing the growth of Cu on W(110) up to the beginning nucleation of the incomplete triplelayer at RT.

where the ratio of island edge to uncovered surface is low.

Apart from the 'fractal chaining' of clusters an additional growth feature, the increase in the diameter of the chains together with a filling of the uncovered areas inside the islands, is visible in Fig. 3. This is accomplished by Cu atoms, which impinge on the substrate within these areas or which initially land on top of the fractal Cu layer and get incorporated at the cluster edge after crossing the step edge.

Fig. 4 shows a growth sequence at RT up to the completion of the first layer and the beginning of the second layer. Three atomic steps of the W substrate cross the images. The influence of these step edges on the growth process results in a preferred nucleation of Cu clusters along the edge. The fractal step flow mode indicates sufficient mobility for the Cu atoms to reach and attach to the W terrace edges within a step width of at least 250 Å at a flux of 1.81×10^{12} atoms $cm^{-2} s^{-1}$. A nucleation of separate islands can be observed at 5–10 times higher Cu fluxes on terraces exceeding a width of about 1000 Å. The distance between such islands and the initial step front is compatible with the determined island density of the unstepped surface in Fig. 3. For the bias voltage of 200 mV chosen in the sequence of Fig. 4 the Cu-covered areas can be distinguished from the initial W step edges due to the geometric contrast caused by the different atomic sizes of Cu and W atoms leading to different corresponding heights of the atomic planes [15]. The boundary remains in the same straight and sharp appearance as seen originally in Fig. 4a, suggesting a lack of any intermixing between W and Cu atoms. This does not change even for 250°C growth as seen in other experiments.

From the in-plane 2D growth of the first fractal Cu layer it is concluded that a significant Schwoebel energy barrier at the single Cu step edge is missing or at least small with respect to the high step edge crossing frequency of the Cu atoms due to the fractal island shape. On the other hand, a quantitative analysis of Fig. 4 and also deposits at 250°C show that the area covered with Cu stripes and islands is approximately proportional to the width of the supporting W terrace.

This proves that in the temperature range between RT and at least 250°C Cu atoms are confined to the terraces on which they initially land, indicating the presence of a significant energy barrier at the boundary between the grown Cu and the initial W terrace edge. In this way, Cu atoms are prevented from crossing from a Cu-covered area to the W substrate lying at the same level, and vice versa. An overcoming of the energy barrier has been reported only for Cu on Mo(110) at higher annealing temperatures, leading to an homogeneous width of Cu stripes at a step edge, irrespective of the terrace width [19]. Jung et al. [19] propose that an explanation of the energy barrier cannot be found exclusively in the weaker bonding of Cu atoms on the Cu-covered area as this only prevents a diffusion from W to Cu due to a potential step. Instead, an effect is suggested to be taken into account which is similar to that one which leads to the formation of the Schwoebel step edge barrier known from homoepitaxy. Thus the assumption of an 'in-plane Schwoebel barrier' in the Cu–W–boundary system appears to be reasonable.

In contrast to Fig. 4 no nucleation of any Cu clusters can be observed at the step edges of Fig. 2. This does not seem to be a consequence of elevated temperature since we observed step edge induced nucleation at temperatures up to 250°C. There are some indications that the azimutal orientation may play a role in the wetting behavior of the step edges. Since we were not able to determine and vary the orientation of the steps precisely it was not possible to study growth at step edges systematically. Moreover, we also cannot exclude contamination by e.g. CO or O, poisoning substrate step edges in some cases and preventing attachment of Cu. It has been shown that even small quantities of CO can alter the growth at step edges completely [20].

From a systematic analysis of Fig. 4 it is evident that an overgrowing of Cu clusters onto neighboring Cu-covered areas, equivalent to the formation of the second layer, is strictly prohibited as long as the first ML has not reached an apparent coverage of about 78% (Fig. 4e). At slightly elevated substrate temperatures this fraction soon approaches 100% as seen from Fig. 2d.

The STM image of the closed first layer shows no periodic structural details. This indicates a pseudomorphic structure (adlayer with a commensurate lattice parameter) which can appear when adsorbate–substrate interactions are of a strength comparable with or higher than the adsorbate–adsorbate interactions [12,21]. Using a model including elastic interactions within the adlayer and a rigid periodic substrate field, Bauer and van der Merwe [12] showed that the growth behavior is determined by the ratio of the neighbor distances in the adlayer to those on the substrate. For a value of 0.933 for Cu on W(110) they predicted pseudomorphism up to the completion of the first ML. Indeed, LEED data ([5] and our own data) show, that the diffraction pattern does not change up to a coverage of 14×10^{14} atoms cm^{-2} (a W(110) plane consists of 14.12×10^{14} atoms cm^{-2}) which confirms that Cu adsorbs in registry with W(110) for the first layer.

3.3. Second layer

The second ML also grows in a fractal geometry by chaining of Cu clusters. However, the initial fractal structure appears to be more densely arranged than in the first layer. The density of nuclei in the second as well as in the next higher layers is clearly lower than that of the first layer, implying a higher mobility of the impinging Cu atoms. We first focus on the feature of small third layer patches which are present on top of the second layer areas right from the beginning. With increasing coverage they join in $[001]_{bcc}$-oriented, quasi-periodically arranged chains (see Fig. 2e–g) indicating that the atomic arrangement of the second layer differs drastically from the first layer.

A detailed examination of the present STM data shows that these third layer patches display a complex behavior depending on the film preparation procedure and cannot be observed under all experimental conditions. The image of Fig. 5a has been taken at RT about 55 min after a higher temperature preparation (about 150°C) of $\Theta=1.71$ ML. In contrast to the time-resolved measurements directly during growth, the third layer chains and patches are nearly completely missing. Instead, a $[001]_{bcc}$-oriented periodic microstructure in form of tiny channels (one-dimensional trench network)

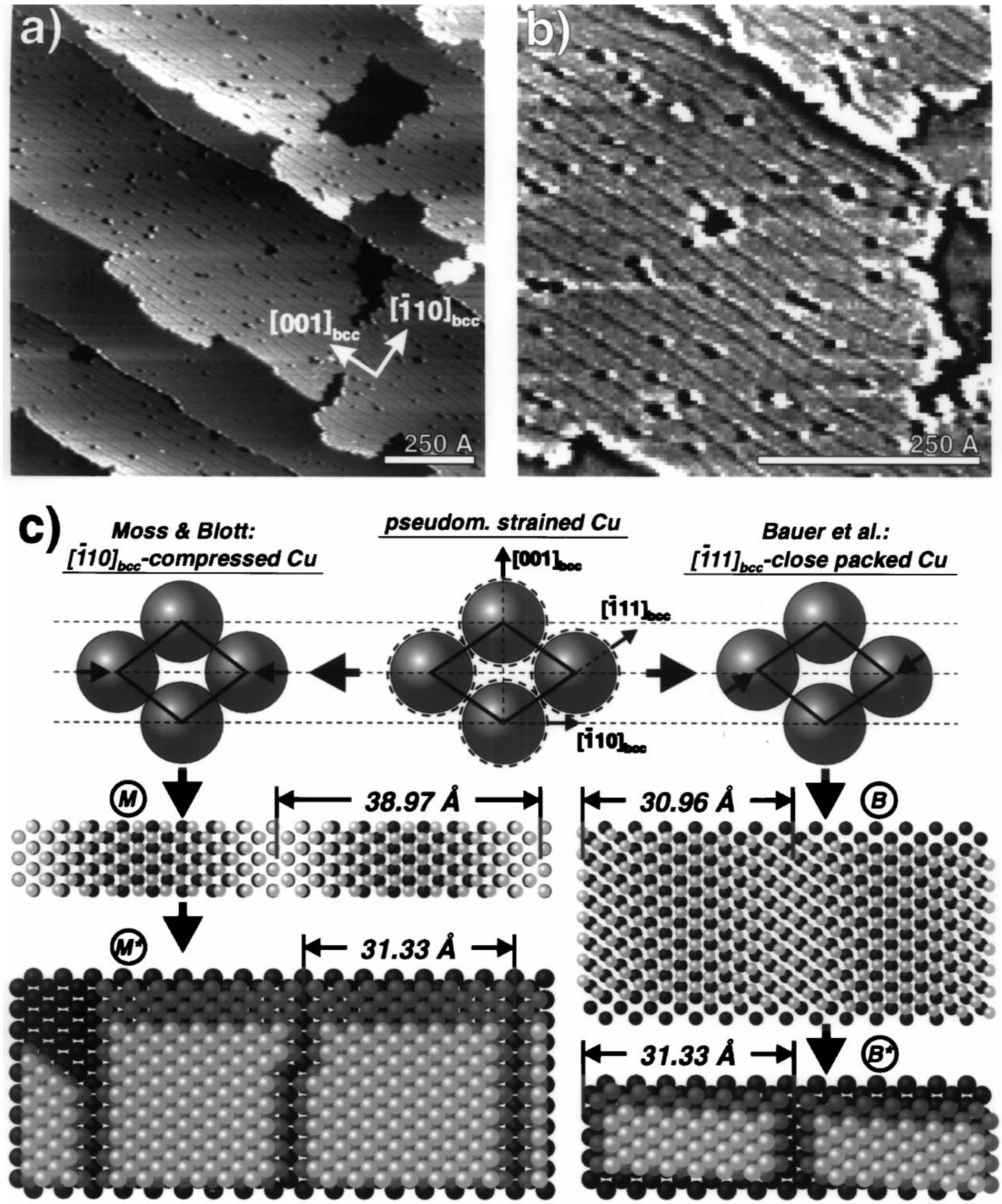

Fig. 5. One-dimensional trench structure of the second layer of Cu on W(110). (a) STM topograph of $\Theta = 1.71$ ML Cu coverage, prepared at $\sim 150°C$, recorded 55 min after growth. (b) Detail of (a) treated by a statistical differencing filter. (c) Two possible structural models for the 2nd layer explaining the trench network, derived from a pseudomorphically strained 1st ML (see text). Cu atoms of the 2nd and 1st layer and W atoms are represented by light, grey and dark circles, respectively. For the nondisrupted epilayer (M and B) the close-packed atom radii have been scaled down by a factor of 0.7 to illustrate the superstructure.

within the second layer can be seen. The third layer chain structure, nucleating at these channels seems to be metastable, staying resident only under a continuous Cu flux during growth. After the growth has stopped and as long as the second layer is incomplete the chains dissolve and the atoms diffuse downwards, leading to a further completion of the second layer. Using a very low Cu flux we have observed a continuous generation and decay of third layer patches on a time scale of seconds. On the other hand, the chain structure together with larger third layer patches remains relatively stable as soon as the second layer is complete (see Fig. 8a). The obviously low binding energy at the third layer patches leads to another effect which could be seen in other time-resolved measurements. During the growth of the fourth layer, a reduction of the third layer chain structure takes place in the immediate proximity of fourth layer islands and especially within vacancies in the fourth layer.

The trench structure in the second layer can be interpreted as a consequence of the fact that above 1 ML of pseudomorphic coverage the Cu–Cu interaction is no longer able to support the large interfacial strain caused by the natural misfit between the W(110) pseudomorphic sites and those of the bulk lattice of Cu. A first incomplete stress relaxation of the film along $[\bar{1}10]_{bcc}$, leads to an extra periodicity in this direction. The closest matched fcc bulk plane of relaxed Cu with regard to the W(110) surface is represented by the fcc Cu(111) plane. Therefore it seems to be remarkable that the relaxation of the second layer takes place in the less strained $[\bar{1}10]_{bcc}$ direction (+1.084%) in comparison with the heavily strained $[001]_{bcc}$ direction (+19.24%) (totally relaxed Cu(111) unit cell in Nishiyama–Wassermann-x orientation with respect to a pseudomorphic Cu cell, see Figs. 1 and 9c). Gollish [23] calculated that the energy surface for an adsorbed Cu atom on W(110) is quite flat in the $[\bar{1}10]_{bcc}$ direction around the normal bcc site (bcc hollow site), see Fig. 1. Therefore, the Cu atoms can move almost freely approximately ± 0.4 Å in the $[\bar{1}10]_{bcc}$ direction to relax. In the perpendicular direction, on the other hand, the energy surface is quite steep preventing an easy relaxation in the $[001]_{bcc}$ direction.

The relaxation of the second layer has previously been observed as LEED satellites (misfit spot splitting, see Fig. 6a) along the $[\bar{1}10]_{bcc}$ direction interpreted as caused by double scattering [5–7]. STM shows that stress relaxation in thermal equilibrium does not result in a coherent periodic dislocation network as seen in the case of Cu on Ru(0001) [22] or Fe on W(110) [24,25], but in a periodically interrupted structure with rows of missing atoms similar to that observed e.g. for Ge on Si(100) [26]. Since we did not achieve atomic resolution on the second layer we propose a model for the atomic arrangement based on an extension of existing models. Two different models have been proposed on the basis of diffraction data assuming a coherent dense epilayer, the first one by Moss and Blott [6], the second one by Bauer et al. [5]. Both models result in a moiré pattern perpendicular to $[\bar{1}10]_{bcc}$. Fig. 5c shows these models together with the modification resulting in a trench structure. The 'Moss and Blott' model (called '$[\bar{1}10]_{bcc}$ compressed Cu' model in Fig. 5c, left) derives from a Cu layer pseudomorphically strained such that the Cu atoms relax in the $[\bar{1}10]_{bcc}$ direction using the Cu hard-sphere diameter of 2.556 Å. Also the 'Bauer et al.' model with two possible domain orientations (called '$[\bar{1}11]_{bcc}$ close packed Cu' model in Fig. 5c, right) derives from a Cu layer pseudomorphically strained by a hard-sphere relaxation. This time the relaxation in the original model is along the $[\bar{1}11]_{bcc}$ direction so that Cu and W atoms are lying in parallel rows along this direction. When the second layer starts to grow the first ML underneath reorganizes simultaneously into the same strained arrangement (so-called distorted fcc (111) layer or approximately (15×1) structure), as clearly seems to be established by LEED [4] and RHEED [8]. In our model the first Cu layer is constructed on top of the W substrate such that sites within the hypothetical moiré structure which are energetically less favored (smaller adsorption energy) are not occupied any longer. In Fig. 5c, M and B, these sites are assumed to be locations in which the Cu atoms are lying more and more above the W atoms. Leaving 4.41 rows along the $[001]_{bcc}$ direction

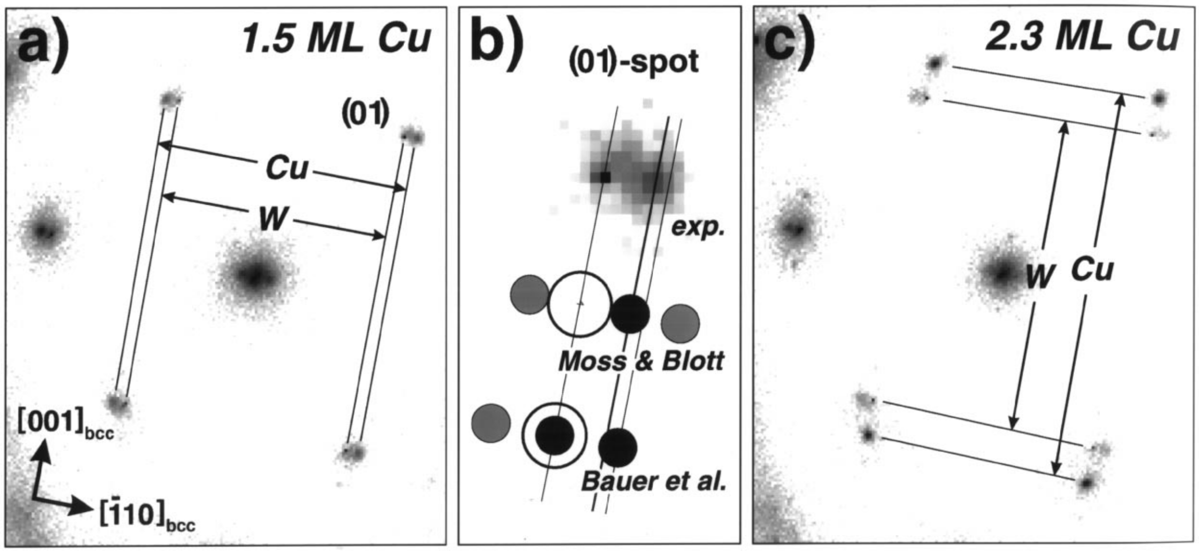

Fig. 6. LEED patterns for Cu on W(110) at RT. (a) $\Theta \approx 1.5$ ML Cu coverage. (b) Comparison of the experimental $[\bar{1}10]_{bcc}$ satellite positions at the (01) spot of (a) with positions for the 'Moss and Blott' and 'Bauer et al.' models. The larger circles represent the (01)–W(110) spot, small black and gray circles are due to scattering from the Cu film and to first order double-scattering from the Cu/W(110) system, respectively. (c) $\Theta \approx 2.3$ ML Cu coverage.

unoccupied for the 'Moss and Blott' model (15 rows remaining) and a 0.83 row for the 'Bauer et al.' model (14 rows remaining) the new period arises as soon as the superstructure fragments are pushed together tightly but commensurately to the underlying W(110) substrate. At the same time a narrow trench as the typical feature of the second layer arises between two such domains. The fact that the domain width is not strictly constant but slightly varying (see Fig. 5b) can be explained by statistical fluctuations in the occupation of the energetically unfavorable edge sites. In the next step, the second ML, which is visible in the STM images, is constructed on top of the rearranged first layer resulting in a reduced number of atoms per domain (13 atom rows in the 'Moss and Blott' model and 12 in the 'Bauer et al.' model) and an expanded trench width. For both models a superstructure period of 31.33 Å defined by the W(110) lattice is formed. With STM we find an average period length of about 31.8 Å which agrees well with both models. In view of a possible preference for one of the proposed models the experimental determination of the atomic density of the double layer which has been carried out by Bauer et al. [5] seems to be less useful, as in both modified models the values are close together and the experimental value of 2.11 ML pseudomorphic coverage (derived from Auger experiments [5]) seems to fit both models if the observed imperfection of the film with a number of vacancies remaining and an additional number of atoms stored in the third layer patches is taken into account. If we assume that the satellites found in LEED are caused by the structure within the domains and not by the period of the trench structure, we can use a precise determination of the relative distance of the outer satellites to the original tungsten spots along the $[\bar{1}10]_{bcc}$ direction (Fig. 6b) in order to compare with the theoretical positions for both possible models. For the modified 'Moss and Blott' model a value of 1.115 is in good agreement with the experimental value of 1.117 ± 0.007 while in the modified 'Bauer et al.' model the value of 1.145 does not fit well. A second fact which supports the modified 'Moss and Blott' model is that in this model the atomic displacement takes place in the $[\bar{1}10]_{bcc}$ direction where an easy displacement is possible (see above) whereas in the modified 'Bauer et al.' model the displacement is rotated by 35.2°.

Therefore, on the present set of data, the modified 'Moss and Blott' model is preferred.

3.4. Third and fourth layers

We now turn to the transition to a nearly relaxed Cu(111) plane in the third and fourth layers. According to the local ordering process of the Cu film a temperature effect can be seen most clearly around the formation of the third layer pattern. The sequence of Fig. 7 shows the evolution of the third layer at RT. Although the growth rate has been chosen to be lower by a factor of 0.2 in comparison with the 80°C measurement shown in Fig. 2, which should enhance the effectiveness of the ordering processes, the layer, in contrast, shows no distinctive formation of third layer chains leading to a disordered arrangement of chain fragments and third layer patches. Less ordered second and first layers are assumed to be the reason. At far higher temperatures, e.g. 300°C (see Fig. 10b), the third layer shows a very well-ordered, nearly perfect equilibrium chain structure (see below), in spite of an even higher growth rate.

Static measurements on a stepped substrate (fig. 8) clearly confirm that both the third and the fourth layer grow simultaneously, as already seen on the upper terrace in the time resolved sequence of Fig. 2. The local terrace width has a strong effect on the coverage distribution between the third and fourth layers: at the same total coverage the fraction of the filled fourth layer is larger for narrow terraces than for broad ones and consequently the coverage of the third layer is reduced. An explanation for this behavior can possibly be found in the increased nucleation density of the fourth layer along a step edge compared with that for the plain terrace. On the other hand, an energetically favored formation of a double layer together with a strong ability for the atoms to interdiffuse between the two layers may also contribute. Disregarding the third layer chains, third and fourth layers therefore tend to grow as a double layer especially pronounced in the case of narrow terraces. An example is given in Fig. 8. The surface area in Fig. 8a consists of terraces with an average width of 277 Å, the one in Fig. 8b of 4 × larger terraces. Although the total coverage is nearly the same, the coverage in the fourth (third) layer is clearly higher (lower) in the case of narrow terraces. Nevertheless, the formation of the fourth layer along a step edge is tied to a nucleation event. Even in the presence of narrow terraces the formation of any fourth layer is delayed if such an event is missing, as seen in the case of hindered step edge wetting on the lower terrace of Fig. 2. From Auger experiments, Bauer et al. [5] concluded (although in contradiction to work function measurements) that the fourth layer only starts to grow after the third layer has completely closed. This would imply very large terraces in their experiments or a case of hindered step edge wetting. We never observed a completely closed third layer before the fourth layer started even on terraces a few thousand Å wide. Another fact which is evident from Fig. 8a is that the total coverage of different terraces is strongly varying (from $\Theta = 2.65$–3.97 ML). This clearly shows that a Schwoebel barrier, separating the coverage on different terraces is not effective any more for the third and fourth layer.

The completion of the third layer without a

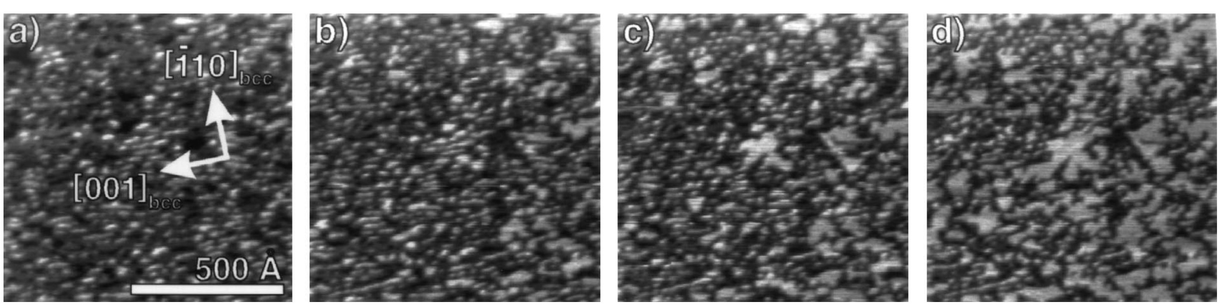

Fig. 7. Sequence of STM images showing the development of the third layer chain structure of Cu on W(110) at RT.

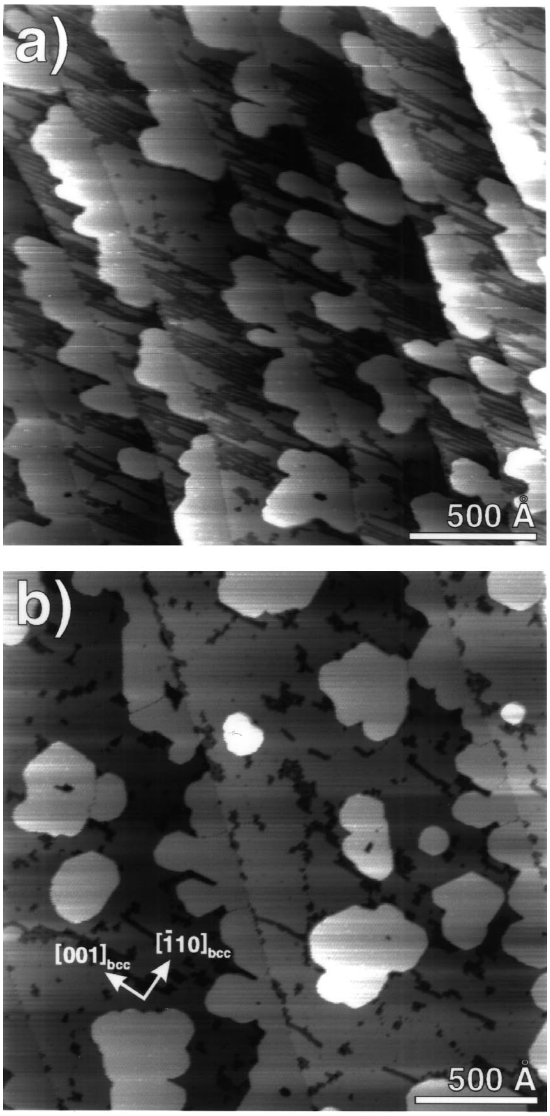

Fig. 8. STM topographs showing the influence of the step density on the growth behavior of the third and fourth Cu layer (see text). Preparation at ~150°C. (a) Average terrace width 277 Å: total coverage $\Theta = 3.04$ ML, $\Theta_{4th} = 0.372$ ML, recorded 80 min after growth. (b) Average terrace width 1120 Å: total coverage $\Theta = 3.22$ ML, $\Theta_{4th} = 0.326$ ML, recorded 175 min after growth.

simultaneous growth of the fourth layer seems to be energetically unfavorable owing to the beginning relaxation to the bulk structure of Cu. The consequences of this second relaxation process can be seen in Fig. 9a,b. Closed areas of the third layer as well as the fourth layer show a one-dimensional dislocation network consisting of lines which are oriented in the $[\bar{1}10]_{bcc}$ direction, rotated by 90° against the trenches in the second layer. Indentations appear at the point where lines meet the edge of the corresponding layer. For the fourth layer the peak-to-peak corrugation amplitude of the structure is 0.25 ± 0.03 Å in the STM images. This value is approximately twice as high as the value 0.11 Å of Xu et al. [9] determined by helium diffraction.

The periodic structure pattern can be explained as a buckling introduced by the incommensurability of the relaxed or nearly completely relaxed Cu film (see later) to the W(110) substrate (rigid lattice approximation). Only the geometries of the two lattices determine the minimum-energy configuration [12]. In our case, the Cu(111) planes are oriented in Nishiyama–Wassermann-x configuration on top of the W(110) substrate [4,12], which means that the $[0\bar{1}1]_{fcc}$ and $[001]_{bcc}$ directions coincide. LEED data of Bauer et al. [5] and own measurements (Fig. 6c) show in this coverage range satellites along the $[001]_{bcc}$ direction which continue to increase in intensity with increasing coverage while the original $[\bar{1}10]_{bcc}$ satellites gradually weaken and finally disappear. Interpreted as caused by double-scattering from the W(110) substrate and the 3–4 layer thick Cu film this diffraction pattern indicates a completely or nearly completely relaxed Cu(111) unit cell in Nishiyama–Wassermann-x orientation, which is consistent with the present STM data. The absence of LEED double-scattering along the $[\bar{1}10]_{bcc}$ direction at coverages of more than four layers indicates that the first two layers also reorganize into Cu(111) planes [4].

Assuming a totally relaxed Cu fcc surface unit cell, the mismatch $(d_{Cu} - d_W)/d_W$ along the $[\bar{1}10]_{bcc}$ axis is only -1.084%. This means that the Cu cell is only slightly smaller than the W cell in this direction. As no corresponding corrugation period of about 408 Å can be observed for large fourth layer areas in the STM images, the Cu cell still seems to be slightly strained in the $[\bar{1}10]_{bcc}$ direction giving an accurate adjustment to the W substrate. Fig. 9c shows a corresponding model. The mismatch of the ideal Cu cell in the $[001]_{bcc}$

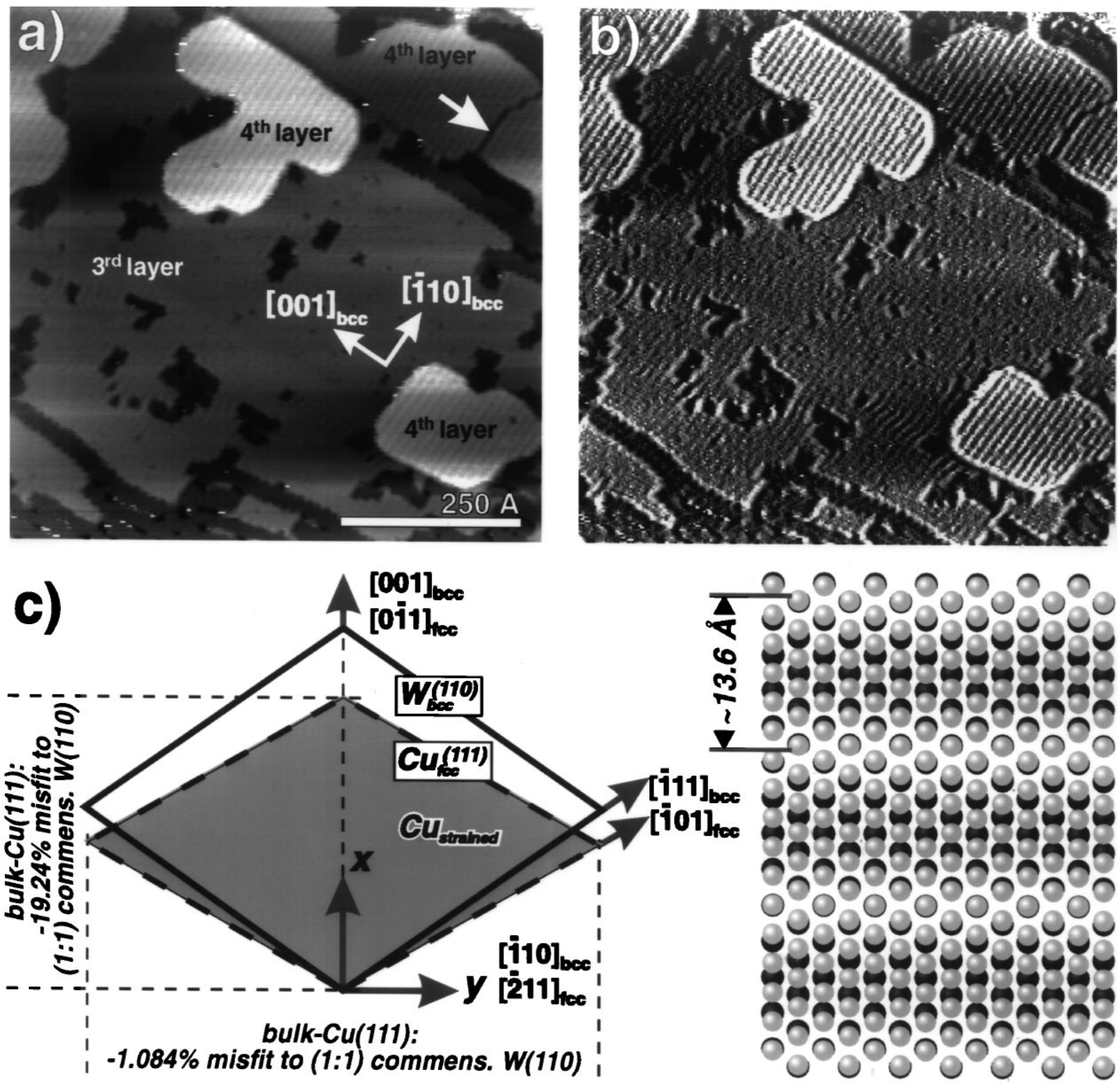

Fig. 9. 1D dislocation network of the third and fourth Cu layer. (a) STM topograph of $\Theta = 3.02$ ML Cu, prepared at $\sim 150°C$, recorded 80 min after growth. (b) Treated by a linear statistical differencing filter. (c) Structural model with a still slightly strained Cu(111) layer in Nishiyama–Wassermann-x Orientation (see text). Cu and W atoms are represented by light and dark circles, respectively. Close-packed atom radii have been scaled down by a factor of 0.7 to illustrate the superstructure.

direction is -19.24% which would lead to a corrugation period of 13.29 Å. This corresponds well to the experimental value of 13.3 ± 0.5 Å from our STM data, while more precise helium diffraction data [9] and our own SPA-LEED (Fig. 6c) data show slightly larger values of 13.6 Å and 13.70 ± 0.18 Å, respectively. According to these values the Cu cell seems to be stretched by $+0.58\%$ also along the $[0\bar{1}1]_{fcc}$ direction compared with the ideal bulk cell. Accordingly, an adjustment to a (5:4) coincidence lattice along the $[001]_{bcc}$ direction, which would be achieved only by a small compression of −0.95%, does not occur. Such a compression could have been expected as the Cu cell is already strained in $[\bar{1}10]_{bcc}$ direction and when there is a tendency to preserve the area of the ideal Cu(111) unit cell.

Within the third layer the periodic corrugation pattern is only weakly ordered. A poorly defined line pattern parallel to the $[\bar{1}10]_{bcc}$ direction is only clearly visible in the neighborhood of holes in the layer. Nevertheless, the pattern seems to be present in the whole third layer as can be seen from the zigzag structure at the island edges. The pattern in the fourth layer is perfectly ordered everywhere. This is an additional indication for a rearrangement of atoms also in deeper layers. Dislocations in the line structure can be observed only occasionally as a hindered coalescence of different fourth layer domains (arrow, Fig. 9a). It could be caused by a different corrugation phase relation between adjacent islands or by a twinning of the close-packed Cu layers (stacking faults).

Even in nearly undistorted areas of the third layer the corrugation pattern is markedly weaker than in the fourth layer. This is surprising because the pattern should fall off only with increasing thickness of the film when the buckling gets more and more smeared out. An electronic effect which has an effect on the STM data acquisition might be responsible. Beyond the fourth layer the line pattern indeed shows a decrease in the corrugation amplitude. For the 5th layer a value of about 4/5 of that of the fourth layer is found.

3.5. Coverages higher than 4 ML

The growth behavior beyond the fourth layer corresponds to the homoepitaxial Cu on Cu growth. The surface roughens with increasing Cu layer thickness pointing to the presence of a Schwoebel barrier in Cu homoepitaxy which cannot be overcome at RT. Nevertheless, the 'heteromorphic' W substrate, which expresses in vacancy defects of the fourth layer, reduces the quality of further epitaxial growth of higher layers. Single fourth layer defects (perhaps also caused by contamination) lead to vacancies in higher layers, as these grow around the corresponding defects. For example, see the point defect in the upper right hand part of Fig. 2m, which closes only in the 8th Cu layer.

3.6. Growth above RT

It is known from the LEED work of Bauer et al. [5] that at elevated deposition temperatures Cu grows in a layer-by-layer mode on W(110) only for two monolayers. STM data (Fig. 10b) clearly prove this behavior. At 300°C and even high Cu coverages of $\Theta \approx 10$ ML the largest part of the surface is covered with a homogeneous double layer of Cu which is decorated with a nearly perfect chain structure (incomplete triplelayer) without closed third layer islands. Defects of this incomplete triple layer are only vacancies within the second layer and a widening of some third layer chains but without the tendency of growing together as seen in the 80°C measurement of Fig. 2. Cu in excess to the incomplete triple layer piles up into three-dimensional fcc crystallites with atomically smooth (111) surfaces even on a misoriented substrate (Fig. 10a, inset) indicating a Stranski–Krastanov growth mode. Depositing thicker Cu layers at RT and annealing at higher temperature leads to a similar topography, formation of Cu crystallites with predominantly (111) planes exposed [5].

We find Cu islands showing diameters larger than 6000 Å in the STM experiment of Fig. 10. The thickness of the wedge-shaped islands exceeds 50 Cu(111) layers and more in the highest parts. The surface of these Cu crystallites exhibits a line pattern in the STM images (Fig. 10a) which apparently is induced by the underlying terrace edges of the stepped W(110) substrate. At this local layer thickness a corrugation network induced by the misfit between substrate and adlayer is not visible even at enhanced grayscale contrast.

3.7. Conclusion

We have shown from an experimental point of view, that STM can provide new information on the system Cu/W(110) even if it has already been analyzed by a number of surface sensitive techniques. When examined in detail, especially time-resolved STM of the growth processes gives new

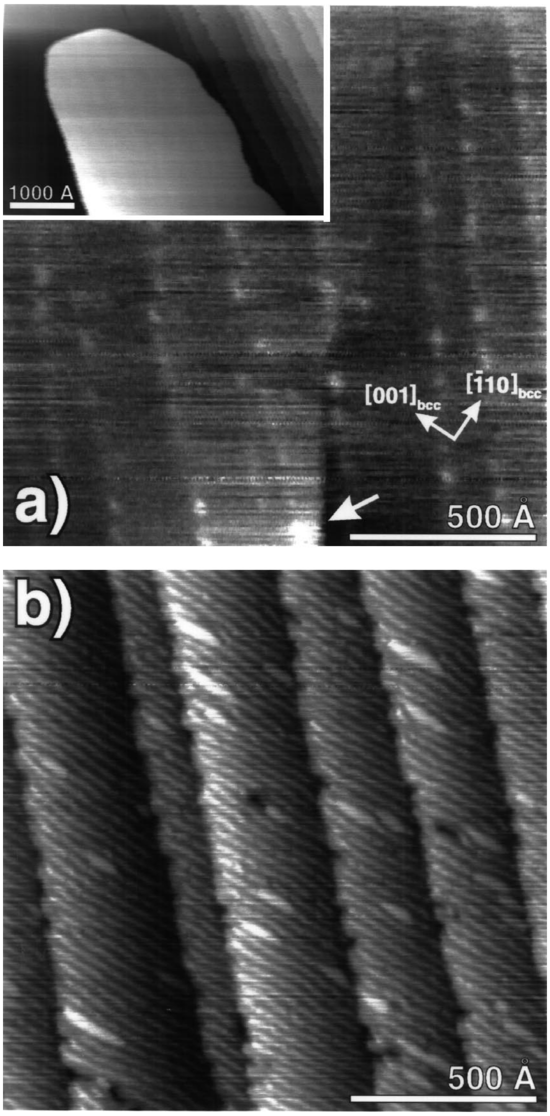

Fig. 10. STM topographs of $\Theta \approx 10$ ML Cu coverage prepared at 300°C. (a, inset) Stranski–Krastanov island surrounded by a low coverage region. (a) On top of a wedge-shaped Stranski–Krastanov island of >40 ML thickness with screw dislocation (the arrow indicates the height of half a 2.087 Å Cu(111) step), recorded 85 min after growth, greyscale from black to white 1.13 Å. (b) Low coverage region showing the well ordered incomplete triple layer, recorded 110 min after growth.

information on nucleation, relaxation and temperature dependent ordering effects of the thin layer.

By stepwise strain relief the relaxation process of Cu on W(110) extends over four layers whereby three different structures related to the first, second and third layers are formed. A detailed insight into the growth mechanisms of the first pseudomorphic layer has been achieved, indicating that the fractal morphology is due to a stress-induced formation of small clusters. In the case of the second layer the basic structure seemed to be quite well understood in the past. STM shows a trench network which can be explained by an extension of existing models. Together with LEED a preference for a modified '$[\bar{1}10]_{bcc}$ compressed Cu' model is possible. The third and fourth layers exhibit a nearly relaxed Cu(111) structure which can be identified clearly by the corrugation pattern found in STM. Together with LEED it is possible to determine a small residual distortion.

For higher coverages and elevated temperatures STM shows the existence of Stranski–Krastanov crystallites coexisting with an incomplete triple layer and therefore confirms earlier assumptions about the growth mode derived indirectly from Auger or LEED.

Acknowledgements

The authors would like to acknowledge the funding by the Deutsche Forschungsgemeinschaft.

References

[1] J.H. van der Merwe, J. Electron Mater. 20 (1991) 793.
[2] E. Bauer, T. Duden, H. Pinkvos, H. Poppa, K. Wurm, J. Magn. Magn. Mater. 156 (1996) 1.
[3] J.C. Lin, N. Shamir, R. Gomer, Surf. Sci. 206 (1988) 61.
[4] E. Bauer, Appl. Surf. Sci. 11–12 (1982) 479.
[5] E. Bauer, H. Poppa, G. Todd, F. Bonczek, J. Appl. Phys. 45 (12) (1974) 5164.
[6] A.R.L. Moss, B.H. Blott, Surf. Sci. 17 (1969) 240.
[7] N.J. Taylor, Surf. Sci. 4 (1966) 161.
[8] G. Lilienkamp, C. Koziol, E. Bauer, Surf. Sci. 226 (1990) 358.
[9] H. Xu, Y. Yang, T. Engel, Surf. Sci. 255 (1991) 73.
[10] H. Poppa, H. Pinkvos, K. Wurm, E. Bauer, Mater. Res. Soc. Symp. Proc. 313 (1993) 219.
[11] E.Z. Luo, Q. Cai, W.F. Chung, B.G. Orr, M.S. Altman, Phys. Rev. B 54 (1996) 14673.
[12] E. Bauer, J.H. van der Merwe, Phys. Rev. B 33 (1986) 3657.

[13] T.A. Witten, L.M. Sanders, Phys. Rev. Lett. 47 (1981) 1400.
[14] T.A. Witten, L.M. Sanders, Phys. Rev. B 27 (1983) 5686.
[15] Y.W. Mo, F.J. Himpsel, Phys. Rev. B 50 (1994) 7868.
[16] M. Paunov, E. Bauer, Appl. Phys. A 44 (1987) 201.
[17] M. Mundschau, E. Bauer, W. Swiech, J. Appl. Phys. 65 (1989) 581.
[18] E. Bauer, Scanning Microsc. 8 (1994) 765.
[19] T. Jung, R. Schlittler, J.K. Gimewski, F.J. Himpsel, Appl. Phys. A 61 (1995) 467.
[20] M. Kalff, G. Comsa, T. Michely, Phys. Rev. Lett. 81 (1998) 1255.
[21] A.D. Novaco, J.P. McTague, Phys. Rev. Lett. 38 (1977) 1286.
[22] G.O. Pötschke, R.J. Behm, Phys. Rev. B 44 (1991) 1442.
[23] H. Gollisch, Surf. Sci. 175 (1986) 249.
[24] H. Bethge, D. Heuer, Ch. Jensen, K. Reshöft, U. Köhler, Surf. Sci. 331–333 (1995) 878.
[25] C. Jensen, K. Reshöft, U. Köhler, Appl. Phys. A 62 (1996) 217.
[26] U. Köhler, O. Jusko, B. Müller, M. Horn-von Hoegen, M. Pook, Ultramicroscopy 42–44 (1992) 832.